

**Fate of the first traversible wormhole: Black-hole collapse or inflationary expansion**

Hisa-aki Shinkai\*

*Computational Science Division, Institute of Physical & Chemical Research (RIKEN), Hirosawa 2-1, Wako, Saitama, 351-0198, Japan*Sean A. Hayward<sup>†</sup>*Department of Science Education, Ewha Womans University, Seoul 120-750, Korea*

(Received 10 May 2002; published 16 August 2002)

We study numerically the stability of the first Morris-Thorne traversible wormhole, shown previously by Ellis to be a solution for a massless ghost Klein-Gordon field. Our code uses a dual-null formulation for spherically symmetric space-time integration, and the numerical range covers both universes connected by the wormhole. We observe that the wormhole is unstable against Gaussian pulses in either exotic or normal massless Klein-Gordon fields. The wormhole throat suffers a bifurcation of horizons and either explodes to form an inflationary universe or collapses to a black hole if the total input energy, is, respectively, negative or positive. As the perturbations become small in total energy, there is evidence for critical solutions with a certain black-hole mass or Hubble constant. The collapse time is related to the initial energy with an apparently universal critical exponent. For normal matter, such as a traveller traversing the wormhole, collapse to a black hole always results. However, carefully balanced additional ghost radiation can maintain the wormhole for a limited time. The black-hole formation from a traversible wormhole confirms the recently proposed duality between them. The inflationary case provides a mechanism for inflating, to macroscopic size, a Planck-sized wormhole formed in space-time foam.

DOI: 10.1103/PhysRevD.66.044005

PACS number(s): 04.70.Bw, 04.25.Dm, 04.40.Nr, 98.80.Cq

**I. INTRODUCTION**

Wormholes are known as a kind of solution to the Einstein equations, and have become a popular research topic, raising theoretical possibilities of rapid interstellar travel, time machines and warp drives. These topics sound like science fiction, but after the influential study of traversible wormholes by Morris and Thorne [1], it became widely accepted as a scientific topic [2]. The only physically nonstandard feature is that one has to assume negative-energy matter to construct such a wormhole. However, such exotic matter occurs extensively in quantum field theory and in alternative gravitational theories such as scalar-tensor theories.

Until recently, wormholes have been studied mainly as static or cut-and-paste models, or without an independently defined exotic matter model. Not long ago, one of the authors [3] proposed a unified theory of black holes and traversible wormholes, arguing that the two are dynamically interconvertible, and that traversible wormholes are understandable as black holes under negative energy density. This opens a new viewpoint on the dynamical nature of both black holes and wormholes, including Hawking radiation. This synthesis has been examined using a low-dimensional model [4], where the theory is affirmed.

The purpose of this article is to investigate wormhole dynamics in four-dimensional Einstein gravity, using numerical simulations. Our starting point is a static wormhole which is perhaps best known as Morris and Thorne's opening example (their box 2). This metric is actually a solution for a massless Klein-Gordon field whose gravitational coupling takes the

opposite sign to normal, as was shown earlier by several authors [5], the earliest of which appears to be Ellis [6], who called it a drainhole. To our knowledge, this is the earliest solution which would nowadays be called a traversible wormhole.

We study dynamical perturbations of this static wormhole, using the spherically symmetric Einstein system with the above exotic matter model, the massless ghost Klein-Gordon field. We developed a numerical code based on a dual-null coordinate system in order to follow the horizon dynamics and radiation propagation clearly. Our main experiment is to add or subtract Gaussian pulses in the ghost field, i.e., respectively, with negative or positive energy. We also consider Gaussian pulses in a normal Klein-Gordon field to see the effect on the wormhole of normal matter, like a human being traversing the wormhole. We discover how the initially static wormhole will change its structure due to these dynamic perturbations. Although our model is specific to spherically symmetric space-times, we believe that it illustrates the dynamical nature of traversible wormholes. To our knowledge, this is the first numerical study of wormhole dynamics.

We describe our model and numerical method in Sec. II and present numerical results in Sec. III. Section IV concludes.

**II. MODEL AND NUMERICAL METHOD****A. Field equations**

The field equations for a massless conventional and ghost Klein-Gordon field,  $\psi$  and  $\phi$ , respectively, in Einstein gravity are, in standard notation,

$$R = 2 \nabla \psi \otimes \nabla \psi - 2 \nabla \phi \otimes \nabla \phi, \quad (2.1)$$

\*Email address: shinkai@atlas.riken.go.jp

<sup>†</sup>Email address: hayward@mm.ewha.ac.kr

$$\square\phi=0, \quad \square\psi=0, \quad (2.2)$$

where the coupling constants have been fixed by choice of units for  $\psi$  and  $\phi$ . We adopt a dual-null formulation developed by one of the authors [7]. The spherically symmetric line-element may be written in dual-null form

$$ds^2=r^2dS^2-2e^{-f}dx^+dx^-, \quad (2.3)$$

where  $dS^2$  refers to the unit sphere. Then the configuration fields are  $(r,f,\phi,\psi)$  as functions of  $(x^+,x^-)$ . The Einstein equations in spherical symmetry are expressed in [8,9], leading to the field equations

$$\partial_{\pm}\partial_{\pm}r+(\partial_{\pm}f)(\partial_{\pm}r)=-r(\partial_{\pm}\psi)^2+r(\partial_{\pm}\phi)^2, \quad (2.4)$$

$$\begin{aligned} r^2\partial_+\partial_-f+2(\partial_+r)(\partial_-r)+e^{-f} \\ =2r^2(\partial_+\psi)(\partial_-\psi)-2r^2(\partial_+\phi)(\partial_-\phi), \end{aligned} \quad (2.5)$$

$$r\partial_+\partial_-r+(\partial_+r)(\partial_-r)+e^{-f}/2=0, \quad (2.6)$$

$$r\partial_+\partial_-\phi+(\partial_+r)(\partial_-\phi)+(\partial_-r)(\partial_+\phi)=0, \quad (2.7)$$

$$r\partial_+\partial_-\psi+(\partial_+r)(\partial_-\psi)+(\partial_-r)(\partial_+\psi)=0. \quad (2.8)$$

To obtain a system accurate near  $\mathcal{I}^{\pm}$ , we can use the conformal factor  $\Omega=1/r$  instead of  $r$  and, as first-order variables, the conformally rescaled momenta

$$\vartheta_{\pm}=2\partial_{\pm}r=-2\Omega^{-2}\partial_{\pm}\Omega, \quad (2.9)$$

$$\nu_{\pm}=\partial_{\pm}f, \quad (2.10)$$

$$\wp_{\pm}=r\partial_{\pm}\phi=\Omega^{-1}\partial_{\pm}\phi, \quad (2.11)$$

$$\pi_{\pm}=r\partial_{\pm}\psi=\Omega^{-1}\partial_{\pm}\psi. \quad (2.12)$$

Here  $\vartheta_{\pm}$  has the meaning of expansion, though it is rescaled from the usual definition,  $\theta_{\pm}=2r^{-1}\partial_{\pm}r$ . Then  $(\wp_{\pm},\pi_{\pm},\vartheta_{\pm},\nu_{\pm})$  are finite and generally nonzero at  $\mathcal{I}^{\pm}$ . The remaining first-order equations follow from the above field equations and the spherically symmetric identity  $\partial_+\partial_-=\partial_-\partial_+$ :

$$\partial_{\pm}\vartheta_{\pm}=-\nu_{\pm}\vartheta_{\pm}-2\Omega\pi_{\pm}^2+2\Omega\wp_{\pm}^2, \quad (2.13)$$

$$\partial_{\pm}\vartheta_{\mp}=-\Omega(\vartheta_+\vartheta_-/2+e^{-f}), \quad (2.14)$$

$$\begin{aligned} \partial_{\pm}\nu_{\mp}=-\Omega^2(\vartheta_+\vartheta_-/2+e^{-f}-2\pi_+\pi_- \\ +2\wp_+\wp_-), \end{aligned} \quad (2.15)$$

$$\partial_{\pm}\wp_{\mp}=-\Omega\vartheta_{\mp}\wp_{\pm}/2, \quad (2.16)$$

$$\partial_{\pm}\pi_{\mp}=-\Omega\vartheta_{\mp}\pi_{\pm}/2. \quad (2.17)$$

These equations plus the inverted momentum definitions

$$\partial_{\pm}\Omega=-\Omega^2\vartheta_{\pm}/2, \quad (2.18)$$

$$\partial_{\pm}f=\nu_{\pm}, \quad (2.19)$$

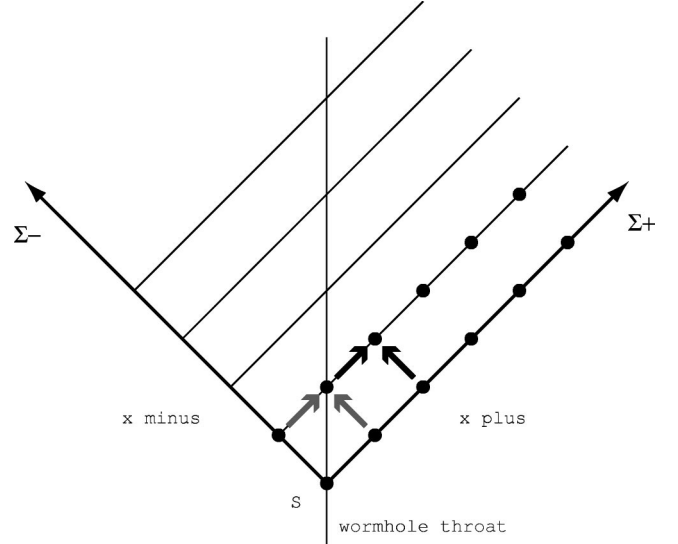


FIG. 1. Numerical grid structure. Initial data are given on null hypersurfaces  $\Sigma_{\pm}$  ( $x^{\mp}=0$ ,  $x^{\pm}>0$ ) and their intersection  $S$ .

$$\partial_{\pm}\phi=\Omega\wp_{\pm}, \quad (2.20)$$

$$\partial_{\pm}\psi=\Omega\pi_{\pm} \quad (2.21)$$

constitute the first-order dual-null form, suitable for numerical coding.

## B. Numerical method

We prepare our numerical integration range as drawn in Fig. 1. The grid will cover both universes connected by the wormhole throat  $x^+=x^-$ . The grid is assumed to be equally spaced in  $\Delta x^{\pm}=\Delta$ .

The basic idea of numerical integration is as follows. We give initial data on a surface  $S$  and the two null hypersurfaces  $\Sigma_{\pm}$  generated from it. Generally the initial data have to be given as

$$(\Omega,f,\vartheta_{\pm},\phi,\psi) \quad \text{on} \quad S:x^+=x^-=0, \quad (2.22)$$

$$(\nu_{\pm},\wp_{\pm},\pi_{\pm}) \quad \text{on} \quad \Sigma_{\pm}:x^{\mp}=0,x^{\pm}>0. \quad (2.23)$$

We then evolve the data  $u=(\Omega,\vartheta_{\pm},f,\nu_{\pm},\phi,\psi,\wp_{\pm},\pi_{\pm})$  on a constant- $x^-$  slice to the next.

Because of the dual-null decomposition, the causal region of a grid is clear, and there are in-built accuracy checks: the integrability conditions or consistency conditions  $\partial_-\partial_+u=\partial_+\partial_-u$ . In order to update a point N (north), we have two routes from the points E (east) and W (west). The set of equations, (2.13)–(2.21), gives us  $x^+$ -direction (W to N) and  $x^-$ -direction (E to N) integrations together with the consistency conditions.

All the equations can be written as

$$u_{new}=u_{old}+f(u_{RHS})\Delta, \quad (2.24)$$

and the input variables,  $u_{\text{RHS}}$ , in the right-hand-side term depend on the integration schemes. In more detail, we followed these steps:

(1) Integrate  $(\Omega, \vartheta_+, \vartheta_-, \nu_-, f, \phi, \psi, \varphi_-, \pi_-)$  using the  $\partial_+$  equations (update N from W): use  $u_{\text{RHS}}=u_W$ ; (2) Integrate  $(\Omega, \vartheta_+, \vartheta_-, \nu_+, f, \phi, \psi, \varphi_+, \pi_+)$  using the  $\partial_-$ -equations (update N from E): use  $u_{\text{RHS}}=u_E$ ; (3) update N from W again: use  $u_{\text{RHS}}=(u_W+u_N)/2$ ; (4) update N from E again: use  $u_{\text{RHS}}=(u_E+u_N)/2$ ; (5) check the consistency of  $(\Omega, \vartheta_+, \vartheta_-, f, \phi)$  at point N. If the convergence is not satisfactory, repeat back to the step 3. We set the tolerance as  $\max|u_{E \rightarrow N} - u_{W \rightarrow N}| < 10^{-5}$  for  $(\Omega, \vartheta_+, \vartheta_-, f, \phi)$ .

As a virtue of the dual-null scheme, we can follow the wormhole throat or black-hole horizons easily. They are both trapping horizons, hypersurfaces where  $\vartheta_+=0$  or  $\vartheta_-=0$  [9,10]. Another benefit is the singular point excision technique. As we described, the causal region of each grid point in the dual-null scheme is apparent. When a grid point is inside a black-hole horizon and near to the singularity, we can exclude that point and grid points in its future null cone from further numerical computation. Actually we excised grid points if one of  $(|\vartheta_+|, |\vartheta_-|, |e^{-f}|)$  exceeds  $\sim 25$ . We found that this is useful for investigating inside a black-hole horizon, though there is naturally a limit on how closely a singularity can be approached.

**C. Static wormhole**

The first Morris-Thorne wormhole metric [1] was given as

$$ds^2 = (a^2 + l^2) dS^2 + dl^2 - dt^2, \tag{2.25}$$

where  $a$  denotes the throat radius of the wormhole. Since it is an overall scale, we set  $a=1$  for numerical purposes but retain it in the text. Transforming the proper radial length  $l$  and the static proper time  $t$  to dual-null coordinates

$$x^\pm = (t \pm l) / \sqrt{2} \tag{2.26}$$

the analytic expressions for the Ellis wormhole solution [6] are

$$\phi = \tan^{-1}(l/a), \tag{2.27}$$

$$\Omega = 1/\sqrt{a^2 + l^2}, \tag{2.28}$$

$$f = 0, \tag{2.29}$$

$$\varphi_\pm = \pm a / \sqrt{2} \sqrt{a^2 + l^2}, \tag{2.30}$$

$$\vartheta_\pm = \pm \sqrt{2} l / \sqrt{a^2 + l^2}, \tag{2.31}$$

$$\nu_\pm = 0 \tag{2.32}$$

with the conventional field  $\psi$  vanishing. The wormhole is symmetric in interchange of the two universes,  $l \rightarrow -l$ , though this will not be so for the perturbations. The energy density is

$$T_{tt} = - \frac{a^2}{8\pi(a^2 + l^2)^2} \tag{2.33}$$

with units  $G=1$ . The negative energy density is a maximum at the throat  $l=0$ , tends to zero at infinity, and is smaller for larger wormholes. Note that the wormhole throat is a double trapping horizon,  $\vartheta_+ = \vartheta_- = 0$ . The behavior of these generally different trapping horizons will be a key indicator of the evolution of the perturbed wormhole.

The dual-null initial data for the static wormhole is

$$(\phi, \Omega, f, \vartheta_\pm) = (0, 1/a, 0, 0) \text{ on } S, \tag{2.34}$$

$$(\varphi_\pm, \nu_\pm) = [\pm a / \sqrt{2a^2 + (x^\pm)^2}, 0] \text{ on } \Sigma_\pm. \tag{2.35}$$

**D. Gravitational mass-energy**

We find that the dynamical structure will be characterized by the total mass or energy of the system, the Bondi energy. Localizing, the local gravitational mass-energy is given by the Misner-Sharp energy  $E$ , while the (localized Bondi) conformal flux vector components  $\varphi^\pm$  were defined in [8,9]:

$$\begin{aligned} E &= (1/2)r[1 - g^{-1}(dr, dr)] \\ &= (1/2)r + e^f r(\partial_+ r)(\partial_- r) \\ &= \frac{1}{2\Omega} \left[ 1 + \frac{1}{2} e^f \vartheta_+ \vartheta_- \right], \end{aligned} \tag{2.36}$$

$$\begin{aligned} \varphi^\pm &= r^2 T^{\pm\pm} \partial_\pm r = r^2 e^{2f} T_{\mp\mp} \partial_\pm r \\ &= e^{2f} (\pi_\mp^2 - \varphi_\mp^2) \vartheta_\pm / 8\pi. \end{aligned} \tag{2.37}$$

They are related by the energy propagation equations or unified first law [9]

$$\partial_\pm E = 4\pi \varphi_\pm = - \frac{1}{2} e^f (\pi_\pm^2 - \varphi_\pm^2) \vartheta_\mp, \tag{2.38}$$

so that one may integrate to

$$E(x^+, x^-) = \frac{a}{2} + 4\pi \int_{(0,0)}^{(x^+, x^-)} (\varphi_+ dx^+ + \varphi_- dx^-), \tag{2.39}$$

where the integral is independent of path, by conservation of energy [8,9]. Here the initial condition  $E|_S = a/2$  corresponds to the static wormhole. The definitions are local, but  $\lim_{x^+ \rightarrow \infty} E$  is the Bondi energy and  $\lim_{x^+ \rightarrow \infty} \varphi_-$  the Bondi flux for the right-hand universe. For the static wormhole, the energy  $E = a^2/2\sqrt{a^2 + l^2}$  is everywhere positive, maximal at the throat, and zero at infinity,  $l \rightarrow \pm\infty$ , i.e., the Bondi energy is zero. Generally, the Bondi energy-loss property, that it should be nonincreasing for matter satisfying the null energy condition [8], is reversed for the ghost field.

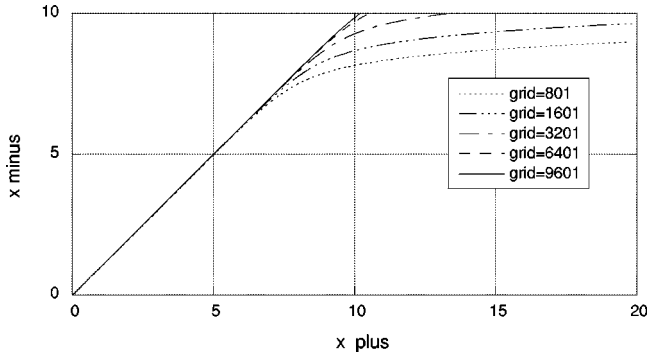


FIG. 2. Convergence behavior of the code for exact static wormhole initial data. The location of the trapping horizon  $\vartheta_- = 0$  is plotted for several resolutions labelled by the number of grid points for  $x^+ = [0, 20]$ . We see that numerical truncation error eventually destroys the static configuration.

### III. DYNAMICAL BEHAVIOR OF TRAVERSIBLE WORMHOLES

#### A. Evolution of a static wormhole

We start with the numerical evolution of the static wormhole. We find that a numerical truncation error can quite easily destroy the stability. In Fig. 2 we show our tracking of the location of the trapping horizon  $\vartheta_- = 0$  for static wormhole initial data, with different numbers of grid points: 801, 1601, . . . , 9601, for  $x^+ = [0, 20]$ . The location of the throat, where  $\vartheta_+ = \vartheta_- = 0$ , is supposed to be stationary at  $x^+ = x^-$ . The figure shows that at sufficient resolution, we can maintain a static wormhole for a given time. Vice versa, this shows that in our dual-null scheme and the current applied numerical integration scheme, the lack of resolution inevitably causes an unstable evolution eventually. We hereafter discuss the dynamical structure of perturbations of the wormhole only in the reliable evolution range, with the resolution kept good enough (9601) to preserve the static case.

In Fig. 3 we demonstrate the numerical evolution of the static wormhole, giving the expansion  $\vartheta_+$  and the local gravitational mass-energy  $E$  as functions of  $(x^+, x^-)$ .

#### B. Gaussian perturbations in ghost field

We first put perturbations of the static wormhole in the form of Gaussian pulses, input from the right-hand universe  $l > 0$ . The initial data on  $\Sigma_+$  is

$$\varphi_+ = a/\sqrt{2}\sqrt{a^2 + l^2} + c_a \exp[-c_b(l - c_c)^2], \quad (3.1)$$

with all other initial data as for the static wormhole. Here  $c_a, c_b, c_c$  are parameters, with runs being performed for increasingly small values of the amplitude  $c_a$ ,  $c_b = 3, 6, 9$  and  $c_c = 3$ . That is, the pulses will hit the wormhole throat at  $x^+ = x^- = 3$ . For  $c_a$  positive or negative, this corresponds, respectively, to enhancing or reducing the supporting ghost field. Note that this pulse-type perturbation starts only from the right-hand universe. This situation is available because our numerical region covers both sides of the wormhole, though we assume that the space-time is locally spherically symmetric.

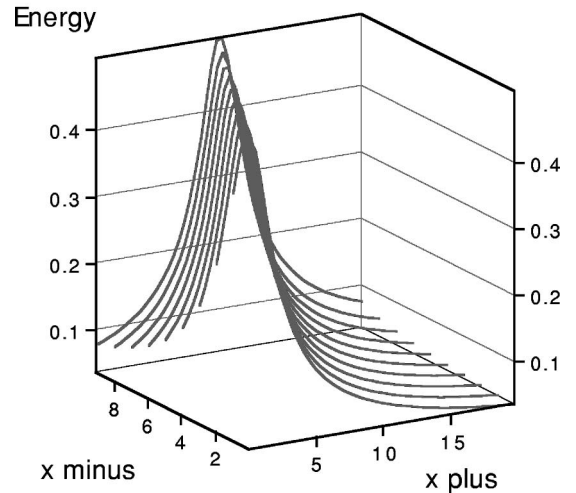
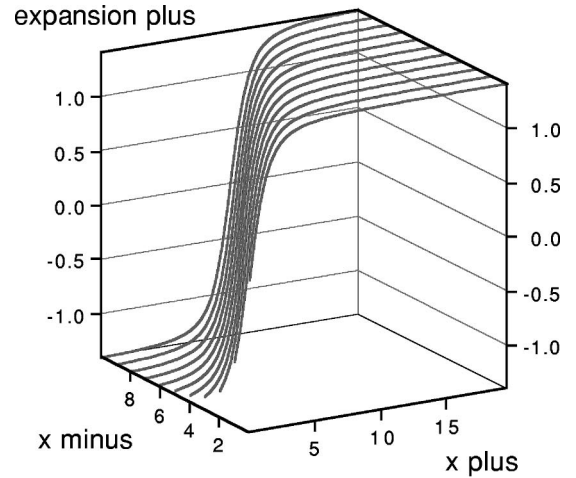


FIG. 3. Static wormhole configuration obtained with the highest resolution calculation: (a) expansion  $\vartheta_+$  and (b) local gravitational mass-energy  $E$  are plotted as functions of  $(x^+, x^-)$ . Note that the energy is positive and tends to zero at infinity.

Figure 4 shows the horizon locations for both  $\vartheta_+ = 0$  and  $\vartheta_- = 0$ , for  $c_b = 3$ . We plotted three cases,  $c_a = \pm 0.1$  and  $-0.01$ , and it can be seen that in each case, the double trapping horizon comprising the initial wormhole throat bifurcates when the pulse hits it. The two horizons then accelerate away from each other, rapidly approaching the speed of light and appearing to be asymptotically null. Due to the grid excision technique for strong curvature regions, the final horizon coordinate  $x_H^-$ , where the right-hand trapping horizon becomes null, is often excised from the numerical computation. In such a case, we determine  $x_H^-$  by extrapolating the horizon trajectory with a function  $x^+ = b_0 + b_1 x^- + b_2 (x^-)^2 + b_3 / (x^- - x_H^-)$ , where  $b_i$  and  $x_H^-$  are unknown constants. A partial Penrose diagram of the evolved space-time is given in Fig. 5, which is like the prediction in [3]. However, the two horizons move in opposite directions depending on the sign of  $c_a$ . In the following, one should bear in mind that  $\vartheta_+ > 0, \vartheta_- < 0$  initially in the right-hand universe  $x^+ > x^-$ , with signs reversing for the left-hand universe.

When we supplement the ghost field,  $c_a = 0.1$ , we see that the  $\vartheta_{\pm} = 0$  horizons move, respectively, in the  $x^{\mp}$  directions,

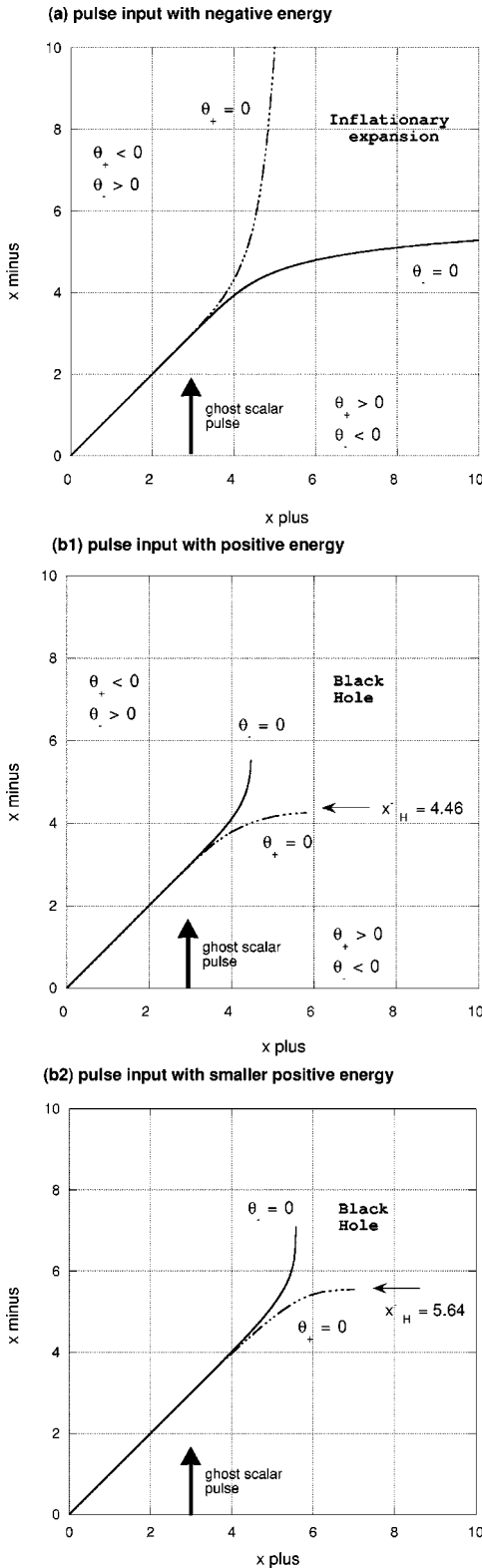


FIG. 4. Horizon locations,  $\vartheta_{\pm}=0$ , for a perturbed wormhole. (a) is the case where we supplement the ghost field,  $c_a=0.1$ , and (b1) and (b2) are where we reduce the field,  $c_a=-0.1$  and  $-0.01$ . Dashed lines and solid lines are  $\vartheta_+=0$  and  $\vartheta_-=0$ , respectively. In all cases, the pulse hits the wormhole throat at  $(x^+,x^-)=(3,3)$ . A 45° counterclockwise rotation of the figure corresponds to a partial Penrose diagram.

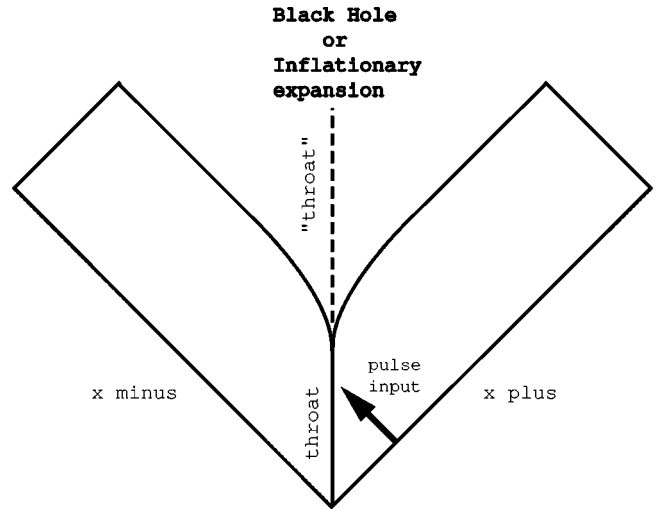


FIG. 5. Partial Penrose diagram of the evolved space-time.

meaning that  $\vartheta_{\pm}>0$  in the region between them. This defines past trapped surfaces, which occur in expanding universes, such as the de Sitter solution. In Fig. 6 we plot the areal radius  $r$  of the “throat” [11]  $x^+=x^-$ , as a function of proper time

$$\tau = \int_{x^+=x^-} e^{-f/2} dt, \quad t = (x^+ + x^-) / \sqrt{2}. \quad (3.2)$$

It can be seen to rapidly increase, actually exponentially: the lines in the figure can be expressed with a function  $r/a = 1 + b_4 \exp[H(\tau - b_5)]$  where  $b_i$  and  $H$  are constants, and we show the Hubble constant  $H$  in Table I. This exponential expansion, combined with the horizon structure, indicates that the wormhole has exploded to an inflationary universe. The two trapping horizons become the cosmological horizons. This connection between wormholes and inflation was unanticipated, but is consistent with the general theory [3].

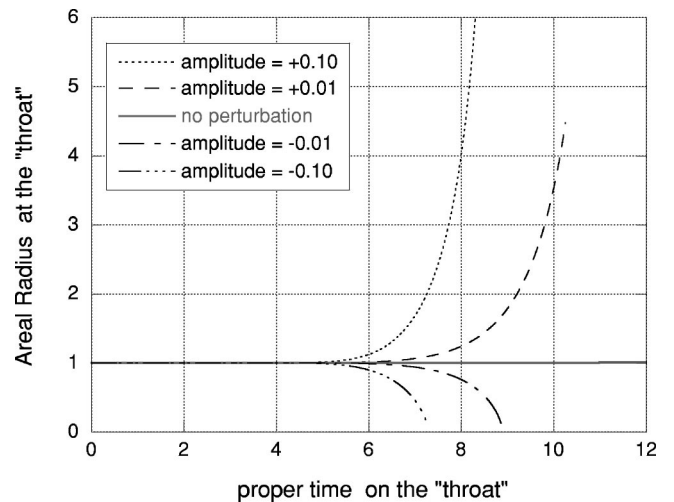


FIG. 6. Areal radius  $r$  of the “throat”  $x^+=x^-$ , plotted as a function of proper time. Additional negative energy causes inflationary expansion, while reduced negative energy causes collapse to a black hole and central singularity.

TABLE I. Initial Bondi energy  $E_0$  and the final structures for different ghost pulse inputs described by Eq. (3.1). The energy is evaluated at  $x^+=20$ , subtracting that of the exact static solution. The final structure was judged at  $x^-=10$  by the horizon structure. For inflation cases, the Hubble constant  $H$  was measured on the ‘‘throat,’’ Fig. 5. For black-hole cases we show the final horizon coordinate  $x_H^-$ , where the  $\vartheta_+=0$  trapping horizon becomes null, Fig. 4(b), and the final mass  $M$  of the black hole, Fig. 7(b).

$c_a$	$c_b$	$E_0/a$	Final structure		
			$Ha$		
$+10^{-1}$	3.0	$-5.07 \times 10^{-2}$	inflation	1.56	[Fig. 4(a)]
$+10^{-2}$	3.0	$-4.45 \times 10^{-3}$	inflation	1.19	
$+10^{-3}$	3.0	$-4.40 \times 10^{-4}$	inflation	1.13	
$+10^{-4}$	3.0	$-4.39 \times 10^{-5}$	inflation	1.12	
0.0	3.0	0.0	static	(Fig. 3)	
$-10^{-4}$	3.0	$+4.39 \times 10^{-5}$	black hole	8.42	0.296
$-10^{-3}$	3.0	$+4.38 \times 10^{-4}$	black hole	6.98	0.310
$-10^{-2}$	3.0	$+4.32 \times 10^{-3}$	black hole	5.64	0.325 [Fig. 4(b2)]
$-10^{-1}$	3.0	$+3.70 \times 10^{-2}$	black hole	4.46	0.420 [Fig. 4(b1)]
$-10^{-1}$	6.0	$+2.60 \times 10^{-2}$	black hole	4.82	0.38
$-10^{-1}$	9.0	$+2.12 \times 10^{-2}$	black hole	4.90	0.35
			$x_H^-/a$	$M/a$	

The two universes connected by the wormhole have essentially been combined into one universe.

On the other hand, when we reduce the ghost field,  $c_a = -0.1$ , the  $\vartheta_{\pm}=0$  horizons move, respectively, in the  $x^{\pm}$  directions, meaning that  $\vartheta_{\pm} < 0$  in the region between them. This defines future trapped surfaces, which occur inside black holes, such as the Schwarzschild solution. Figure 6 shows that the areal radius is heading towards zero in finite proper time, though the code cannot follow it into the apparent central singularity. This and the horizon structure indicates that the wormhole has collapsed to a black hole. The trapping horizons appear to become asymptotically null, where they would coincide with the event horizons of the black hole. This occurs around  $x_H^- \sim 4.46$  for the right-hand universe.

If the amplitude of the pulse is reduced, the black hole forms later, as shown in Fig. 4(b2) for  $c_a = -0.01$ . As a physical measure of the size of the perturbation, we take the initial Bondi energy

$$E_0 = E(\infty, 0) \tag{3.3}$$

scaled by the initial throat radius  $a$ . In practice we take  $E(20, 0)$  and subtract the corresponding value for the static wormhole. Some data are presented in Table I. We find that positive  $E_0$  will cause collapse to a black hole, while negative  $E_0$  will cause explosion to an inflationary universe. Also, the speed of the horizon bifurcation increases with the energy. One could also scale the total energy by the maximal initial energy  $E$ , but this occurs at the throat and is  $a/2$ . In either case, the perturbations are small, down to 1% in en-

ergy, yet the final structure is dramatically different. Thus we conclude that the static wormhole is unstable.

Accepting that the static wormhole is stable to linear perturbations [12,13], we seem to have discovered a nonlinear instability, something of interest in itself. Circumstantial evidence for a quadratic instability is that it is first signalled by nonzero values of  $\nu_{\pm}$ , and the propagation equations (2.15) for  $\nu_{\pm}$  have quadratic terms on the right-hand side, which should cancel to zero in the static solution. This could be addressed by second-order perturbation theory, but we know of no such studies for wormholes.

In Fig. 7 we plot the energy  $E(x^+, x^-)$  as a function of  $x^-$ , for  $x^+ = 12, 16, 20$  for the three cases in Fig. 4. In each case, the mass increases rapidly in  $x^-$  as the horizon  $\vartheta_{\pm} = 0$  forms, but rapidly approaches a constant value in  $x^+$  at the horizon. This value

$$M = E(\infty, x_H^-) \tag{3.4}$$

is the final mass of the black hole. Obtaining this easily is another virtue of the dual null scheme. The values are shown in Table I. The graphs indicate that an observer at infinity will see a burst of radiation as the wormhole collapses or explodes. For collapse, a certain fraction of the field energy radiates away, the rest being captured by the black hole, constituting its mass. For explosion, the radiated energy continues to rise in an apparently self-supporting way as the universe inflates.

Figure 8 gives a survey of various parameters of  $c_a$  and  $c_b$ , fixing  $c_c = 3$ . Figure 8(a) shows how quickly the black-hole horizon, the outer trapping horizon  $\vartheta_+ = 0$ , develops after the pulse hits the throat. We see that the dots are close to one line, indicating a logarithmic relation between the collapse time and the initial energy of the perturbation,

$$e^{x_H^- - 3} \propto E_0^{-0.60}. \tag{3.5}$$

Figure 8(b) is the final black hole mass  $M$  as a function of the initial energy of the perturbation. Interestingly, as the perturbations become small, the black-hole mass seems to approach a nonzero constant,

$$M \sim 0.30a. \tag{3.6}$$

In the inflationary case, the Hubble parameter  $H$  (or horizon mass  $1/2H$ ) also seems to have a limiting value for small perturbations, as seen in Table I:

$$H \sim 1.1/a. \tag{3.7}$$

Since these masses are the same order as the wormhole scale  $a$ , we guess that the static wormhole is something like an instanton with two different attractors nearby. This scenario requires more detailed study with different models, and we plan to report it subsequently.

### C. Gaussian pulses in conventional field

Similarly, we next consider adding a small amount of conventional scalar field to the static wormhole solution. This is

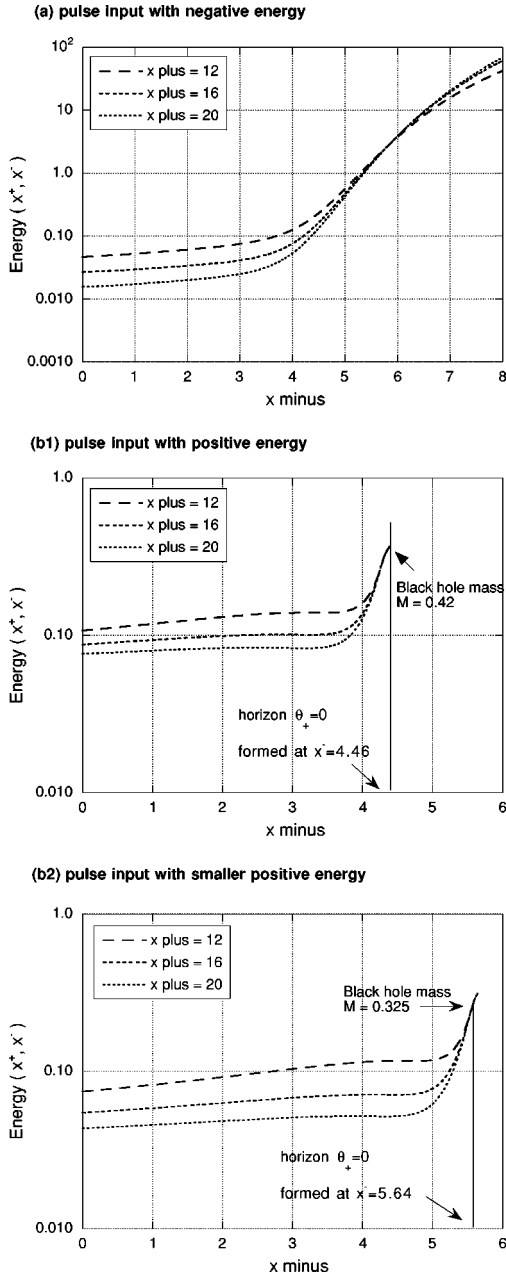


FIG. 7. Energy  $E(x^+, x^-)$  as a function of  $x^-$ , for  $x^+ = 12, 16, 20$ . Here  $c_a$  is (a) 0.05, (b1)  $-0.1$ , and (b2)  $-0.01$ . The energy for different  $x^+$  coincides at the final horizon location  $x_H^-$ , indicating that the horizon quickly attains constant mass  $M = E(\infty, x_H^-)$ . This is the final mass of the black hole. The values are shown in Table I.

a simplified model of a situation that a positive-energy creature jumps into a traversible wormhole. Again we add Gaussian pulses to the initial data on  $\Sigma_+$  as

$$\pi_+ = \tilde{c}_a \exp[-\tilde{c}_b(l - \tilde{c}_c)^2], \quad (3.8)$$

with all other initial data as for the static wormhole. We set  $\tilde{c}_b = \tilde{c}_c = 3$ , so that the pulse will again hit the wormhole throat at  $x^+ = x^- = 3$ .

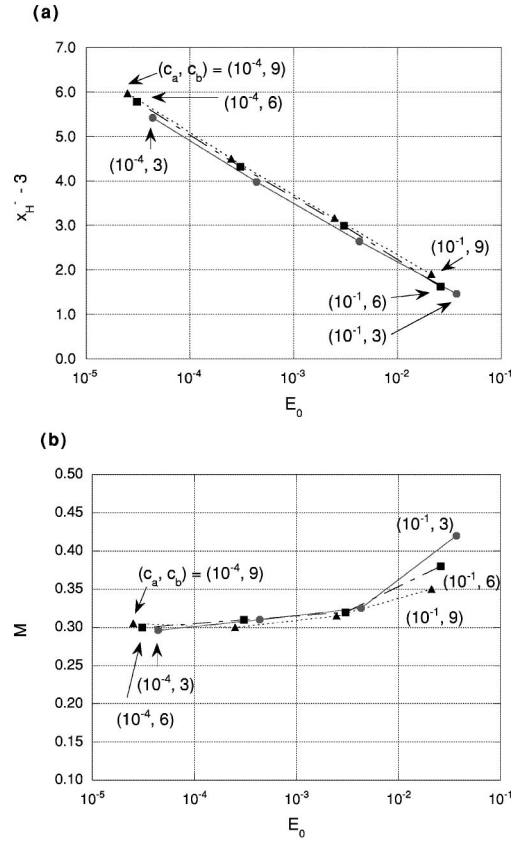


FIG. 8. Relation between the initial perturbation and the final mass of the black hole. (a) The final horizon ( $\vartheta_+ = 0$ ) coordinate  $x_H^- - 3$ , since we fixed  $c_c = 3$ , versus initial energy of the perturbation,  $E_0$ . We plotted the results of the runs of  $c_a = 10^{-1}, 10^{-4}$  with  $c_b = 3, 6$ , and  $9$ . They lie close to one line. (b) The final black hole mass  $M$  for the same examples. We see that  $M$  appears to reach a nonzero minimum for small perturbations.

We show the horizon structure in Fig. 9 and initial total energy in Table II. The additional normal field slightly enhances the total energy, with either sign of amplitude, and the wormhole collapses to a black hole. The fundamental dynamical behavior is the same as for the previous ghost perturbations with positive energy. We see again a logarithmic relation between the time and the initial energy of the perturbation,  $e^{x_H^- - 3} \propto E_0^{-0.61}$ , Fig. 10(a). The critical exponent is consistent with that found for perturbations in the ghost field, indicating a new kind of critical behavior reminiscent of that found by Choptuik [14] in black-hole collapse. In the limit of small perturbations, the black-hole mass also appears to approach the same nonzero constant,  $M \sim 0.30a$ , Fig. 10(b). Although the current code has a limit on how small perturbations can be, since the black-hole collapse should occur within the reliable evolution range, the data suggest the existence of a critical solution with a certain black-hole mass.

For these perturbations, the energy perturbation is as small as about 0.01%, a quite convincing indication of instability. From this and general principles [3], we expect that any normal matter traversing the wormhole will cause its collapse to a black hole.

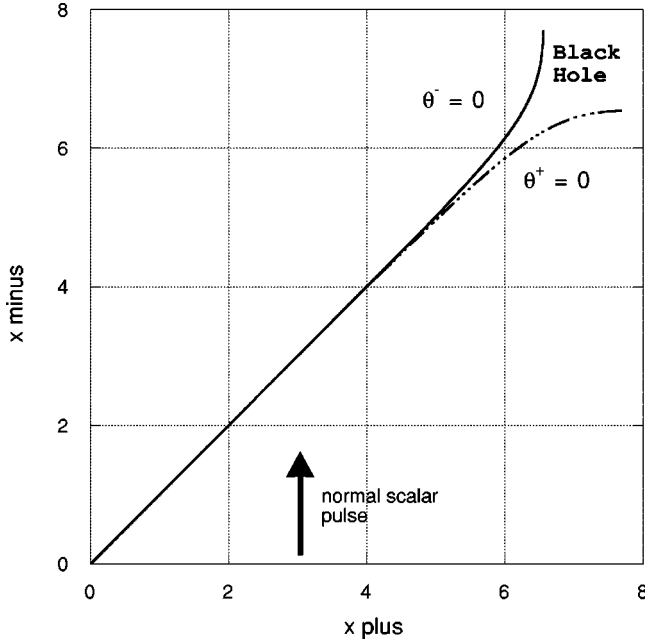


FIG. 9. Evolution of a wormhole perturbed by a normal scalar field. Horizon locations: dashed lines and solid lines are  $\vartheta_+ = 0$  and  $\vartheta_- = 0$ , respectively.

#### D. Wormhole maintenance

Supposing the normal field pulse represents an actual traveller of the traversible wormhole, then he, she, or it may go through the wormhole and exit safely into the other universe if the speed is high enough, as can be seen from the Penrose diagram obtained from Fig. 9. However, the wormhole itself will collapse to a black hole, ending its usefulness for travellers.

We here demonstrate a kind of temporary maintenance of the wormhole by sending in an additional ghost pulse just after the passing of the traveller. In Fig. 11 we show the results for pulse parameters  $(\tilde{c}_a, \tilde{c}_b, \tilde{c}_c) = (0.1, 6.0, 2.0)$  for the normal field representing the traveller, combined with a balancing pulse  $(c_a, c_b, c_c) = (0.023\ 90, 6.0, 3.0)$ , case B, or  $(c_a, c_b, c_c) = (0.023\ 85, 6.0, 3.0)$ , case C. If we do not send the balancing pulse, the wormhole collapses to a black hole with horizons given by case A in the plot. Case B ends up with an inflationary expansion, while case C keeps the wormhole structure at least until  $x^- = 10$ . Since the final fate of the wormhole is either a black hole or an inflationary

TABLE II. Initial Bondi energy  $E_0$  and the final structures for different conventional pulse inputs described by Eq. (3.8). The columns are the same as for Table I.

$\tilde{c}_a$	$\tilde{c}_b$	$E_0/a$		$x_H^-/a$	$M/a$
$\pm 1 \times 10^{-2}$	3.0	$+6.86 \times 10^{-5}$	black hole	9.61	0.31
$\pm 5 \times 10^{-2}$	3.0	$+1.71 \times 10^{-3}$	black hole	7.50	0.32
$\pm 1 \times 10^{-1}$	3.0	$+6.86 \times 10^{-3}$	black hole	6.68	0.34 (Fig. 9)
$\pm 5 \times 10^{-1}$	3.0	$+1.71 \times 10^{-1}$	black hole	4.82	0.46
$\pm 1 \times 10^0$	3.0	$+6.86 \times 10^{-1}$	black hole	3.70	0.90

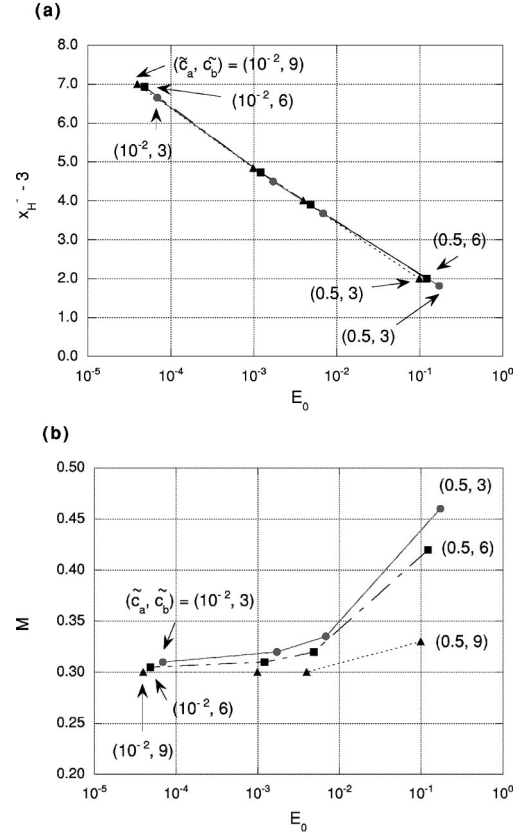


FIG. 10. The same plots as in Fig. 8 for conventional field pulses. (a) The final horizon ( $\vartheta_+ = 0$ ) coordinate  $x_H^- - 3$  versus initial energy of the perturbation,  $E_0$ . We plotted the results of the runs of  $\tilde{c}_a = 0.5, \dots, 10^{-2}$  with  $\tilde{c}_b = 3, 6$ , and 9. They lie close to one line, different to that of Fig. 8(a), but with the same gradient. (b) The final black hole mass  $M$  for the same examples.

expansion, to keep the throat as it was requires a fine-tuning of the parameters, and may not be realistic. However, it shows how the wormhole life may be extended. This indicates that the wormhole might be maintained by continual adjustments to the radiation level, though it would be a never-ending project.

#### IV. DISCUSSION

We have numerically studied the dynamic stability of the apparently earliest [6] and most frequently rediscovered [3,5] traversible wormhole, most famous as the first Morris-Thorne wormhole [1]. We observe that the wormhole is unstable against Gaussian pulses in both exotic and normal massless Klein-Gordon fields. The wormhole throat suffers a bifurcation of horizons and will either explode to an inflationary universe or collapse to a black hole if the total energy is, respectively, negative or positive. For the normal matter, the total energy is necessarily positive and a black hole always results. This black-hole formation from a traversible wormhole confirms the unified theory of both [3].

The inflationary expansion provides a mechanism for enlarging a quantum wormhole to macroscopic size. Wheeler introduced wormholes to gravitational physics as part of his still-popular idea of space-time foam [15], which envisages

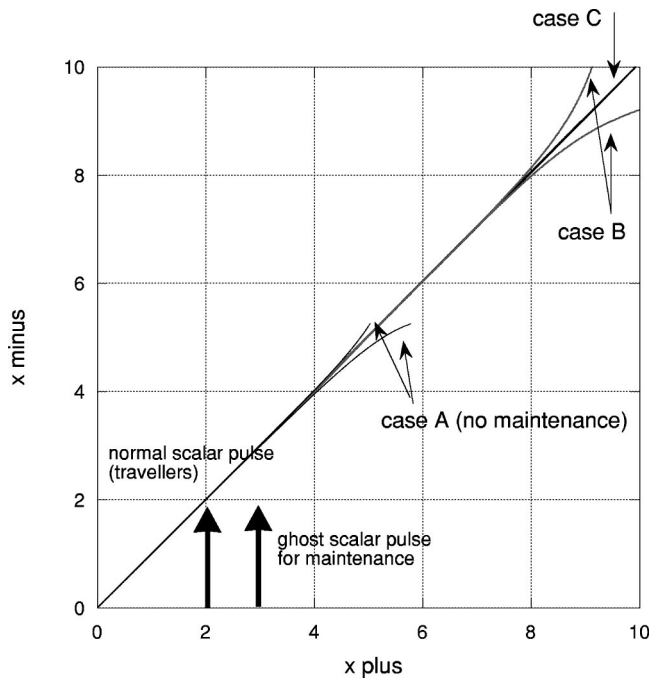


FIG. 11. Temporary wormhole maintenance. After a normal scalar pulse representing a traveller, we beamed in an additional ghost pulse to extend the life of the wormhole. Horizon locations  $\partial_+ = 0$  are plotted for three cases: (A) no maintenance, which results in a black hole; (B) with a maintenance pulse which results in an inflationary expansion; (C) with a more finely tuned maintenance pulse, which keeps the static structure up to the end of the range.

transient wormholes at the Planck scale, due to quantum fluctuations in space-time topology. Morris and Thorne imagined pulling a wormhole out of this foam and enlarging it somehow. Actual mechanisms are scarce: Roman [16] suggested inflation, though without an independently defined exotic matter model, and Redmount and Suen [17] found a quantum-mechanical instability of certain cut-and-paste wormholes in a space-time foam model, also leading to unbounded expansion. We have discovered that for one of the simplest classical exotic matter fields, wormholes can natu-

rally inflate. The problem is only to stop the inflation proceeding indefinitely.

The results also provide an entertaining answer to the question of what happens if someone attempts to traverse the wormhole. At best, with sufficient alacrity, our hero could exit into the other universe, only to look behind and see that the passage has caused the wormhole to collapse to a black hole, thereby sealing off the causal connection to the home universe. Perhaps there was also an unlucky companion who did not make it through, suffering the well-known grisly fate of being trapped in a black hole. The survivor would be left to ruminate on the ironic fate of those who would tamper with the fabric of space-time: stranded forever in the twilight zone. As we showed, such a tragedy could be avoided by a carefully calculated burst of ghost radiation, just before or after the traveller passes, which maintains the static wormhole for a certain time. The traveller then has a limited time to explore the other universe before the wormhole collapses.

For our colleagues who are understandably sceptical about wormholes and exotic matter, we hope that our numerical study has at least demonstrated that they can be studied and understood by the same local, dynamical methods as used for black holes with normal matter. Indeed, the results lead straight back to mainstream physics of black holes and inflation, with new discoveries about both, particularly the apparent critical behavior. For a general audience, perhaps the message is that (albeit theoretical) science can be stranger than science fiction.

#### ACKNOWLEDGMENTS

H.S. would like to thank Y. Eriguchi, Y. Kojima, T. Harada, and M. Shibata for comments, and S-W. Kim for hospitality in visiting Ewha Womans University. S.A.H. would like to thank S-W. Kim, S. Sushkov, K. Bronnikov, and C. Armendariz-Picon for discussions. H.S. is supported by the special postdoctoral researchers program at RIKEN, and this work was supported partially by the Grant-in-Aid for Scientific Research Fund of Japan Society of the Promotion of Science, No. 14740179. S.A.H. is supported by Korea Research Foundation grant KRF-2001-015-DP0095.

- [1] M.S. Morris and K.S. Thorne, *Am. J. Phys.* **56**, 395 (1988).
- [2] M. Visser, *Lorentzian Wormholes* (AIP Press, New York, 1995).
- [3] S.A. Hayward, *Int. J. Mod. Phys. D* **8**, 373 (1999).
- [4] S.A. Hayward, S.-W. Kim, and H. Lee, *Phys. Rev. D* **65**, 064003 (2002).
- [5] G. Clément, *Am. J. Phys.* **57**, 967 (1989).
- [6] H.G. Ellis, *J. Math. Phys.* **14**, 395 (1973).
- [7] S.A. Hayward, *Class. Quantum Grav.* **10**, 779 (1993).
- [8] S.A. Hayward, *Phys. Rev. D* **53**, 1938 (1996).
- [9] S.A. Hayward, *Class. Quantum Grav.* **15**, 3147 (1998).
- [10] S.A. Hayward, *Phys. Rev. D* **49**, 6467 (1994).
- [11] Once the wormhole is perturbed, this hypersurface loses its

- specific geometrical meaning as the wormhole throat  $l=0$ . However, one can say that it is composed of minimal surfaces in some family of spatial hypersurfaces, which are locally close to the constant- $t$  family for small perturbations.
- [12] K.A. Bronnikov, G. Clément, C.P. Constantinidis, and J.C. Fabris, *Phys. Lett. A* **243**, 121 (1998).
- [13] C. Armendariz-Picon, *Phys. Rev. D* **65**, 104010 (2002).
- [14] M.W. Choptuik, *Phys. Rev. Lett.* **70**, 9 (1993).
- [15] J.A. Wheeler, *Ann. Phys. (N.Y.)* **2**, 604 (1957).
- [16] T.A. Roman, *Phys. Rev. D* **47**, 1370 (1993).
- [17] I.H. Redmount and W.-M. Suen, *Phys. Rev. D* **47**, 2163 (1993).